Stabilization by Configurational Entropy of the Cu(II) Active Site During CO Oxidation on $Mg_{0.2}Co_{0.2}Ni_{0.2}Cu_{0.2}Zn_{0.2}O$

Journal:	*The Journal of Physical Chemistry Letters*
Manuscript ID	jz-2020-00602d.R1
Manuscript Type:	Letter
Date Submitted by the Author:	n/a
Complete List of Authors:	Fracchia, Martina; Universita degli Studi di Pavia, Dipartimento di Chimica Ghigna, Paolo; Università di Pavia, Dipartimento di Chimica Fisica Pozzi, Tommaso; Università di Pavia, Dipartimento di Chimica, Università degli Studi di Pavia Anselmi-Tamburini, Umberto; Universita degli Studi di Pavia, Chemistry Colombo, Valentina; Universita degli Studi di Milano, Department of Chemistry Braglia, Luca; Istituto Officina dei Materiali Consiglio Nazionale delle Ricerche, TASC Laboratory Torelli, Piero; Istituto Officina dei Materiali Consiglio Nazionale delle Ricerche, TASC Laboratory

Stabilization by Configurational Entropy of the Cu(II) Active Site during CO Oxidation on $Mg_{0.2}Co_{0.2}Ni_{0.2}Cu_{0.2}Zn_{0.2}O$

Martina Fracchia[1], Paolo Ghigna[1,2], Tommaso Pozzi[1], Umberto Anselmi Tamburini[1,2], Valentina Colombo[2,3], Luca Braglia[4], Piero Torelli[4]*

[1]Dipartimento di Chimica, Università di Pavia, V.le Taramelli 13, I-27100, Pavia, Italy
[2]INSTM, Consorzio Interuniversitario per la Scienza e Tecnologia dei Materiali, Via Giusti 9, 50121 Firenze, Italy
[3]Dipartimento di Chimica, Università degli Studi di Milano, Via Golgi 19, I-20133, Milano, Italy.
[4]CNR- Istituto Officina dei Materiali, TASC, Trieste, Italia

AUTHOR INFORMATION

Corresponding Author

*Paolo Ghigna, Dept. Chemistry, University of Pavia, V.le Taramelli 13, I-27100, Pavia, Italy.

Email: paolo.ghigna@unipv.it; Tel. +390382987574; FAX: +390382987575.

ABSTRACT

The mechanisms of CO oxidation on the $Mg_{0.2}Co_{0.2}Ni_{0.2}Cu_{0.2}Zn_{0.2}O$ high entropy oxide were studied by means of operando soft X-ray absorption spectroscopy. We found that Cu is the active metal, and that Cu(II) can be rapidly reduced to Cu(I) by CO when the temperature is larger than 130 °C. Co and Ni do not have any role in this respect. The Cu(II) oxidation state can be easily but slowly recovered by treating the sample in O_2 at *ca.* 250 °C. However, it should be noted that CuO is readily and irreversibly reduced to Cu(I) if treated in CO at T>100 °C. Thus, the main conclusion of this work is that the high configurational entropy of $Mg_{0.2}Co_{0.2}Ni_{0.2}Cu_{0.2}Zn_{0.2}O$ stabilizes the rock-salt structure and permits the oxidation/reduction of Cu to be reversible, thus permitting the catalytic cycle to take place.

TOC GRAPHICS

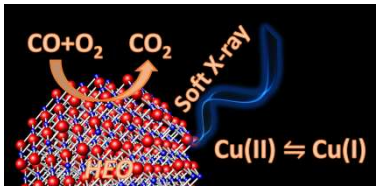

KEYWORDS: High Entropy Oxides, Operando Soft-XAS, Mechanisms of Heterogeneous Catalysis, Oxidation of CO.

Low-temperature CO oxidation, perhaps the most extensively studied reaction in the history of heterogeneous catalysis, is becoming increasingly important in the context of cleaning air and lowering of the automotive emissions[1]. Hopcalite catalysts (manganese and copper spinel) were originally developed for purifying air in submarines, but they are not particularly active at ambient temperatures and are also deactivated by the presence of moisture[2]. Noble metal catalysts, on the other hand, are water tolerant but usually require temperatures above 100 °C for efficient operation[3]. Gold exhibits high activity at low temperatures and superior stability under moisture, but only when deposited as nanoparticles on transition-metal oxides[4]. The development of active and stable catalysts without noble metals for low-temperature CO oxidation under ambient atmosphere remains a significant challenge. Among the metal oxides, the Co_3O_4 spinel is the most active for CO oxidation[5], but is severely deactivated by trace amounts of moisture (about 3–10 ppm) that are usually present in the feed gas. In fact, under dry conditions with a moisture content below 1 ppm, which can be obtained by passing the reaction gas through molecular-sieve traps cooled to dry-ice temperature, Co_3O_4 is intrinsically active for CO oxidation[6] even below a temperature of –54 °C. However, in normal feed gas, most of the active sites of Co_3O_4 are covered by H_2O, so the adsorption of CO and oxygen is appreciably hindered. Alumina-supported Co_3O_4 was reported to give 50% CO conversion at -63 °C for a normal feed gas, but the CO conversion was obtained with a transient method[7] rather than at steady state. Mechanistic studies show that CO molecules interact preferably with the surface Co^{3+} cation, which is the only favourable site for CO adsorption, as confirmed both theoretically[8] and experimentally[9] . The oxidation of the adsorbed CO then occurs by extracting the surface oxygen that might be coordinated with three Co^{3+} cations. This rationale suggests that the presence of transition metals in high oxidation state

is a prerequisite for finding effective catalysts for the CO oxidation reaction; indeed, all the oxide catalysts for the CO oxidation reaction do have metals in high or mixed oxidation or valence states. In this context, the recent discovery of a noticeable catalytic activity of the High Entropy Oxide (HEO) $Mg_{0.2}Co_{0.2}Ni_{0.2}Cu_{0.2}Zn_{0.2}O$, which has a rock-salt structure, towards the CO oxidation reaction[10] is quite surprising, as all the cations are formally in the ME(II) oxidation state. HEOs are a recently discovered class of materials[11] where a particular crystal structure, that is in general different from that of the parent compounds, is stabilized in a multicomponent system (generally, 5 or more) by the large amount of configurational entropy[12]. The main driver for the growing interest in HEOs is the potential to obtain novel properties by exploiting the enormous number of possible elemental combinations; in addition, the synthesis of these materials is facile, and several synthetic routes can be explored for obtaining highly reproducible materials.

As previously mentioned, the catalytic activity of the $Mg_{0.2}Co_{0.2}Ni_{0.2}Cu_{0.2}Zn_{0.2}O$ HEO at quite low temperatures (250-300 °C) towards the CO oxidation reaction poses a series of questions concerning the mechanisms of the catalytic circle, as none of the parent oxides has such a reactivity. The questions mainly concern the local electronic structure of the transition metals (Co, Ni, Cu and Zn), their oxidation states, the nature of the active surface site, and possible changes of all these properties thereof during the reaction course. We here plan to tackle this problem by operando soft X-ray absorption spectroscopy (Soft-XAS) experiments at the transition metals (TM) $L_{2,3}$-edges. In the recent years, in situ and operando investigations at L-edges of transition metals are receiving increasing attention in the field of catalysis[13-15.] In fact, soft-XAS in the total electron yield (TEY) mode combines two unique features: i) the capability of directly monitoring the density of empty 3*d* states for TMs when the $L_{2,3}$ edges are selected, and ii) the surface sensitivity which, due to the low value of electron escape depth, limits the thickness of the probed

sample to few atomic layers below the surface. More details on the choice of soft-XAS as a mechanistic tool for this catalytic reaction can be found in the Supporting Information.

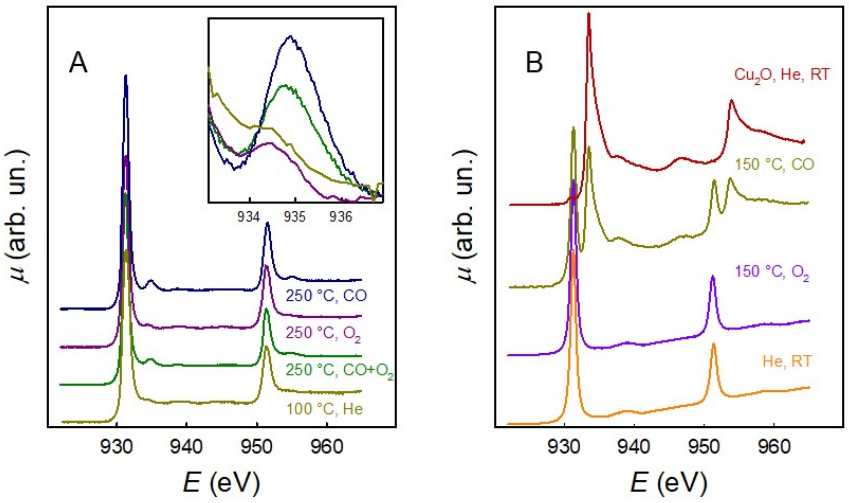

Figure 1 – A: Cu $L_{2,3}$-edge XAS spectra of the $Mg_{0.2}Co_{0.2}Ni_{0.2}Cu_{0.2}Zn_{0.2}O$ HEO material in different conditions. The inset shows on an enlarged scale the Cu(I) peak at *ca.* 934.8 eV. B: Cu $L_{2,3}$-edge XAS spectra of CuO in different conditions and of Cu_2O at room temperature. In this panel, non-normalised spectra are shown.

Fig. 1 shows the Cu $L_{2,3}$-edge XAS spectra of the HEO in different conditions. Spectra of CuO and Cu_2O are also shown for a better reference. The spectrum of CuO presents a clear, intense peak at both the L_3 and L_2 edges, due to electronic transitions from $2p$ to the empty $3d$ states of the d^9 electronic configuration of Cu(II)[16]. The interpretation of Cu_2O spectrum is more complex, as Cu(I) is formally in the d^{10} electronic configuration and therefore the $2p \rightarrow 3d$ electronic transitions would be in principle impossible. However, there is a general consensus that Cu(I) in linear coordination in Cu_2O gives rise to an unusually large partial $3d$ character in the empty density of states.[16,17] In any case, it is clear that, while the peak at the L_3-edge at *ca.* 931.3 eV is

attributed to Cu(II), the peak at the L_3-edge at *ca.* 934.8 eV is a clear signature of Cu(I). We can now discuss the Cu $L_{2,3}$ spectrum of the $Mg_{0.2}Co_{0.2}Ni_{0.2}Cu_{0.2}Zn_{0.2}O$ HEO. At room temperature and in inert gas, the spectrum bears a close resemblance to that of CuO; this is reasonable, due to the fact that, in the HEO with the rock-salt structure, Cu(II) has an octahedral environment similar to that of CuO[11]. It should also be noted that the Cu $L_{2,3}$-edge spectrum can be properly reproduced by multiplet calculations using an undistorted octahedral Cu(II) model with a d^9 configuration (see Supporting Information, Figure S1).

When heating the sample at *ca.* 250 °C in the stoichiometric $CO+1/2O_2$ gas mixture, a peak at *ca.* 934.8 eV starts to appear, as apparent in the green curve in Fig. 1; this, according to the above discussion, is the signature of Cu(I). At this temperature, the CO_2 gas sensor shows that the CO oxidation has reached the maximum rate (see Supporting Information, Fig. S2). The Cu(I) peak amplitude can be reduced by stopping the CO flow and flowing only oxygen on the sample (dark pink line in Fig. 1). This result shows unequivocally that the CO oxidation on the HEO proceeds via adsorption of CO on the Cu sites at the surface. This adsorption causes a charge transfer from CO to Cu, thus leading to Cu(I). Then, if the temperature is high enough to allow the oxidation of adsorbed CO by O_2, CO_2 leaves the surface and some Cu(I) is reoxidised to Cu(II). The finding that the presence of some Cu(I) is found when the oxidation reaction takes place is consistent with the fact that the reduction is faster than the oxidation. It should be noted that the reduction/oxidation of Cu takes place at *ca.* 130 °C, that is well below the temperature at which the CO oxidation rate, as measured by the CO_2 sensor, begins to be significant (see Supporting Information, Fig. S3). This may be attributed to the fact that additional activation energy is required for the oxidation of the adsorbed CO. The fractions of Cu(I) at 250 °C, in the $CO+1/2O_2$ gas mixture and in CO, can be estimated to be 3 and 8 %, respectively (see Fig. S4 and Tab. S1 for

further details). Charge compensation of the Cu'_{Cu} defects that are created by Cu(II) reduction can be achieved by formation of oxygen vacancies.

Ni and Co, the two other metals of the system that are not in a closed shell electronic configuration, act as spectators. We cannot detect any change at the Ni and Co $L_{2,3}$-edges, as shown in Fig. 2, which displays the Ni and Co $L_{2,3}$-edge XAS spectra in similar conditions with respect to those at the Cu $L_{2,3}$-edge shown in Fig. 1. It is well evident that no changes are detected; moreover, the spectra show a very close resemblance with the Ni $L_{2,3}$-edge spectrum of NiO[18], and with the Co $L_{2,3}$-edge spectrum of CoO[19].

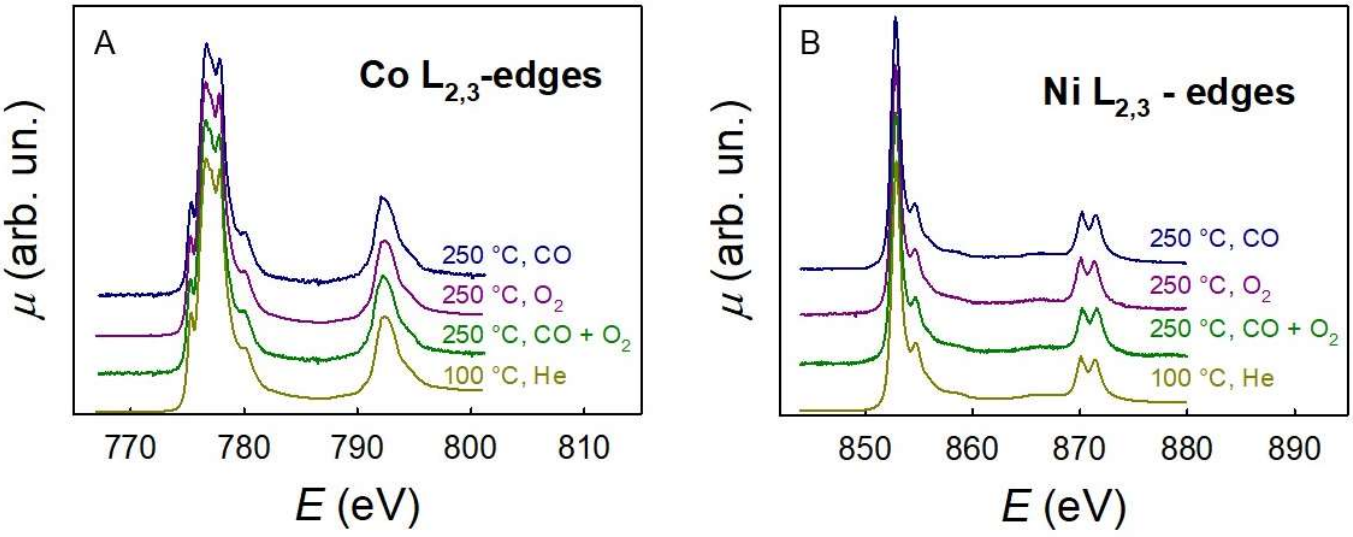

Figure 2 – A: Co $L_{2,3}$-edge XAS spectra of the $Mg_{0.2}Co_{0.2}Ni_{0.2}Cu_{0.2}Zn_{0.2}O$ HEO material in different conditions. T. B: same as A but at the Ni $L_{2,3}$-edge.

As for the spectra at the Cu $L_{2,3}$-edge, the similarity with the corresponding ME(II) oxides is due to the fact that in the HEO the transition metals are in an octahedral environment and in the ME(II) oxidation state. Also in this case, the spectra are well interpreted by multiplet calculations using an undistorted octahedral Me(II) model (see Supporting Information, Fig. S1).

The HEO is quite stable towards reduction. In fact, heating at *ca.* 250 °C in CO (blue line in Fig. 1) the intensity of the Cu(I) peak at *ca.* 934.8 eV increases. However, we should remark that pure copper oxide, CuO, is heavily reduced to Cu(I) when treated in flowing CO at *T* as low as 150 °C, as shown in Fig. 1B. This evidence is important as it emphasises the role of the configurational entropy of the HEO material in stabilising the Cu(II) oxidation state. This fact is indeed very notable, as it may open the way to the tailoring of new catalytic materials by stabilising unstable oxidation states via the configurational entropy concept. To further investigate this fact, we heated the HEO sample at 235 °C in O_2 and then we switched the flowing gas to CO, keeping the sample at the same temperature for 1 h. The results are shown in Fig. 3.

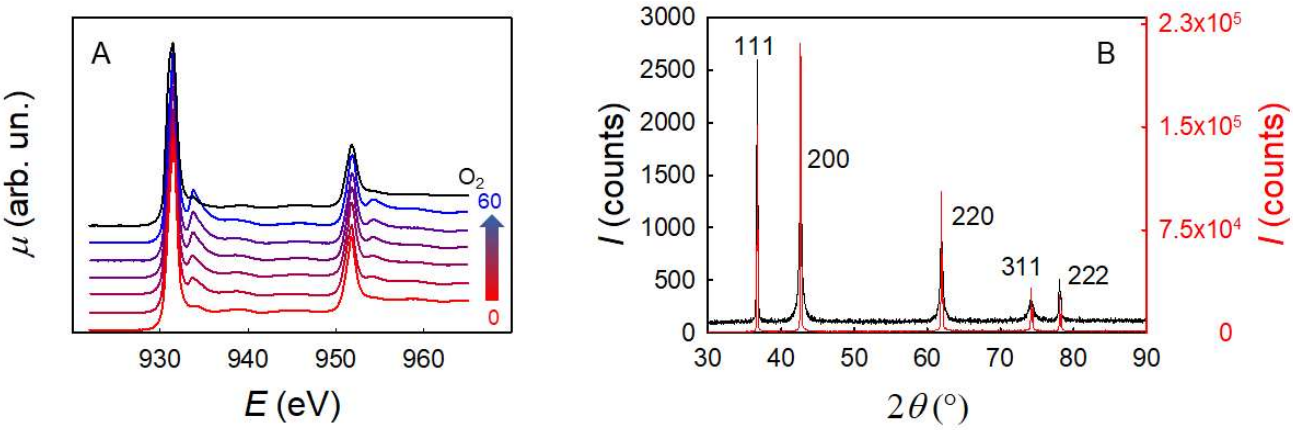

Figure 3 – A: Cu $L_{2,3}$-edge XAS spectra of the $Mg_{0.2}Co_{0.2}Ni_{0.2}Cu_{0.2}Zn_{0.2}O$ HEO material for different time periods in CO at 235 °C (red to blue lines; numbers 0 → 60 are the dwell times in these conditions expressed in minutes), and then in O_2 at the same temperature (black line). B: comparison of the XRPD pattern of the raw HEO material (red line) and of the same material after all the thermal treatments described in this work (black line). The patterns are indexed according to the rock-salt structure (*Fm-3m*, a = 4.2366(5) Å).

The spectra show an increasing intensity of the Cu(I) peak at *ca.* 934.8 eV with increasing time in CO. After 1 h, the gas flow was switched back to O_2: this lead to a considerable reduction of the intensity of the Cu(I) peak at *ca.* 934.8 eV, adding further confirmation to the role of configurational entropy in stabilising the Cu(II)/Cu(I) redox couple. It should be noted that the effects of these thermal treatments on the HEO structure are non-trivial. This is illustrated in Fig. 3B, where the diffraction patterns of the as-prepared HEO is compared with that of the material as taken out of the soft-XAS operando cell. It is well apparent that, while the overall rock-salt structure is preserved, as confirmed by the absence of any additional diffraction effect, all the reflections, bar the 111 family, display a considerable broadening after the thermal treatments.

This is somewhat in agreement with the role of copper ions in HEO rock-salts samples, which has been demonstrated to unambiguously promote the structural evolution from an *ideal* rock-salt to a *distorted* one in copper containing samples *vs.* copper-free ones.[20] Rietveld analysis performed on the as-synthetized sample show that all Bragg peaks are indeed indexed in the rock-salt $Fm\bar{3}m$ space group and that their relative intensities well matches with a random distribution of the cations for the *ideal* rock-salt of $Mg_{0.2}Co_{0.2}Ni_{0.2}Cu_{0.2}Zn_{0.2}O$ composition (see Supporting Information). After the thermal treatments and the changing in oxidation state of copper ions, the broadening of the $(200)_c$, $(220)_c$ and $(311)_c$ peaks nicely corresponds to a tetragonal distortion to the non-isomorphic subgroup *I4*/*mmm* (*a*, 2.9919(2); *c*, 4.2520(4) Å). However, a concomitant presence of a lattice deformation *(i.e.* loss of long-range ordering, perpendicularly to the $(111)_c$ direction) cannot be excluded. The details of this phenomenon are currently under investigation by our group, for a deeper understanding of the observed peak broadening. Indeed, an EXAFS study on this material revealed a considerable local distortion of the Cu-O octahedron, probably driven by Jahn-Teller distortion around the Cu(II) in the d^9 electronic configuration[21]. On the other hand, also

Co(II) and Ni(II), with the d^7 and d^8 configuration, respectively, are Jahn-Teller cations, and, in addition, Zn is known to preferentially assume the tetrahedral coordination with oxygen with respect to octahedral. Finally, in the HEO structure, each of the metal-oxygen distance is forced by the crystal symmetry to be different with respect to that implied by considering the local environment only. We can speculate, therefore, that in the HEO structure, several "*distortion fields*" are present around each of the cations, and the final crystal symmetry is the result of a perfect cancellation of these fields. Removing or altering one of these fields, for example changing the oxidation state of Cu, and therefore changing the electronic configuration from d^9 to d^{10}, and then removing the Jahn-Teller distortion, would result as a net distortion of the whole crystal.

In summary, in this work we investigated the mechanisms of CO oxidation on the $Mg_{0.2}Co_{0.2}Ni_{0.2}Cu_{0.2}Zn_{0.2}O$ high entropy oxide with the rock-salt structure. We found that the only metal involved in the reaction is Cu, while Ni and Co act as spectators. Cu(II) is reduced to Cu(I) by the reactive adsorption of CO. Oxygen can then oxidize the adsorbed CO, forming CO_2 and recovering the Cu(II) oxidation state. The rock salt structure of HEO may therefore have a crucial role in stabilising the redox Cu(II)/Cu(I) couple. On the other hand, the most thermodynamically stable polymorph of CuO shows a monoclinic structure, different from cubic rock salt. Stabilisation of rock-salt CuO therefore requires additional terms to the Gibbs free energy. Rock salt CuO can indeed be prepared in form of nanoparticles, in turn showing a lower reactivity towards reducing gases when compared to the monoclinic polymorph[22]. For nanoparticles, additional terms to the Gibbs free energy result from surface or interfacial contributions. As it is made apparent by the diffraction patterns shown in Fig. 3 B, the $Mg_{0.2}Co_{0.2}Ni_{0.2}Cu_{0.2}Zn_{0.2}O$ HEO material investigated in this work displays very large crystallites: this allow to exclude that surface or interfacial terms play an active role in our case. Thus, we are left with the conclusion that

configurational entropy $S_{config} = -R\sum_i \chi_i ln\, \chi_i$, where χ_i are the molar fractions of the constituents *i*, is the stabilising contribution to the Gibbs free energy for the rock-salt structure of HEO, and it is therefore here responsible of the permanence of Cu(II). This last observation can be of extreme importance as it paves the way for a novel strategy for stabilisation of materials with elements in exotic and/or unstable oxidation states.

A final comment concerns the possibility of using the $Mg_{0.2}Co_{0.2}Ni_{0.2}Cu_{0.2}Zn_{0.2}O$ HEO material as a real catalyst for the CO oxidation reaction. The above result and literature data[10] show that the HEO is active at temperatures that are well above RT. On the other hand, as already mentioned in above, oxide catalyst for the CO oxidation reaction such as Co_3O_4 are inactivated by moisture, and therefore need to be activated before the reaction. We did not observed any deactivation for the HEO, and we could perform the reaction directly on the as prepared powder without any preliminary treatment. This indicates that the HEO is resistant towards contaminations by moisture. In addition, it should be noted that the large crystals formed by the HEO material used in the present investigation limit the surface area to relatively small values. The possibility of preparing the HEO in form of nanoparticles is currently under investigation by our group, as a starting basis for a complete investigation of the catalytic performance of this material, aiming at lowering the working temperatures.

EXPERIMENTAL METHODS

Synthesis and characterization

Crystalline $Mg_{0.2}Co_{0.2}Ni_{0.2}Cu_{0.2}Zn_{0.2}O$ was prepared by a sol-gel route starting from metal nitrates. All the reagents were purchased at analytical grade from Sigma-Aldrich and were used without

further purification. The nitrates were dissolved in water and then citric acid was added (1:1 molar ratio). The reaction mixture was stirred for 12 h at 80 °C, and then dried in an oven at 120 °C for 2 h. The resulting powder was then grinded with an agate mortar and pestle and calcined for 2 h at 900°C, and then quenched to room temperature in air. The chemical and phase purity was then checked by X-ray powder diffraction (XRPD).

X-ray powder Diffraction Analysis

Gently ground powders of $Mg_{0.2}Co_{0.2}Ni_{0.2}Cu_{0.2}Zn_{0.2}O$ were deposited in the, 2 mm deep, hollow of a zero background plate (a properly misoriented quartz monocrystal). Diffraction experiments were performed using Cu-Kα radiation (λ = 1.5418 Å) on a vertical-scan Bruker AXS D8 Advance diffractometer in θ:θ mode, equipped with a Goebel Mirror and a Bruker Lynxeye linear Position Sensitive Detector (PSD), with the following optics: primary and secondary Soller slits, 2.3° and 2.5°, respectively; divergence slit, 0.1°; receiving slit, 2.82°. Generator setting: 40 kV, 40 mA. The nominal resolution for the present set-up is 0.08° 2θ (FWHM of the α1 component) for the LaB_6 peak at about 21.3° (2θ). The accurate diffraction pattern at RT of $Mg_{0.2}Co_{0.2}Ni_{0.2}Cu_{0.2}Zn_{0.2}O$ before and after the reaction was acquired in the 10–105° and 10-90 2θ range, respectively, with Δ2θ = 0.02° and exposure time 2 s/step. Further details on the Le Bail and Rietveld refinements are reported in the Supporting Information.

XAS experiment

For the XAS experiment, a small amount of the $Mg_{0.2}Co_{0.2}Ni_{0.2}Cu_{0.2}Zn_{0.2}O$ material (5 mg *ca.*), in form of loose powder, was hand pressed on the sample holder of the reaction cell of the APE beamline at the ELETTRA synchrotron radiation facility. The sample holder is fixed with screws onto the titanium base of the cell, which is floating from ground and connected with a coaxial cable. In this geometry, the X-ray beam passes through the membrane and the gas layer, then hits

the sample and generates the secondary emission, which is collected by a picoammeter connected to the sample and measuring the drain current. All the measurements were performed keeping the sample grounded through the picoammeter and applying a positive bias voltage of 40 V to the membrane. The cell is mounted in the UHV chamber of the APE-HE beamline, coaxially with the X-ray beam. The reaction cell was mounted on an x-y table that allows its movement in the plane perpendicular to the incident beam with 5 μm vectorial precision. This allows the alignment of the membrane on to the beam. The sample surface, inside the cell, sits in the focal point of the beamline[23]. The measurements were performed at the Co, Ni and Cu $L_{2,3}$-edges. Surface sensitivity is obtained by collecting the XAS spectra ion total electron yield mode: the estimated probed depth is ca. 3-4 nm[24]. To ensure for maximum gas purity, especially concerning water and carbon oxides, the He carrier gas was passed through a liquid N_2 trap before entering the cell. The spectra at all the edges have been background subtracted by fitting the pre-edge with a straight line, and then normalised to unit absorption after the L_3 edge, although explicitly stated that non-normalised spectra are shown. The experiments were conducted in flowing He (50 standard cubic centimeter per minute, SCCM), either pure or with the addition of CO (2 SCCM), O_2 (2 SCCM), or with the stoichiometric CO+O_2 mixture (2+1 SCCM, respectively). All gases were supplied by Linde, with a purity of at least 99.999 %. The CO_2 concentration in the exhaust pipeline of the APE operando cell was measured by means of a non dispersive infrared CO_2 sensor (Gravity, Dfrobot SEN0219). The sensor was completely embedded in the gas flowing out of the reaction cell, and its response was converted in CO_2 concentration by means of a National Instrument data acquisition interface, after calibration with a standard (Linde, 99.999 %). The sensor output, transformed in fraction of converted CO, is shown in Fig. S2, and it is in good agreement with previous reports[10]. Multiplet

calculations were performed by means of the XTM4XAS program[25], including crystal field, charge transfer and spin orbit-coupling effects.

ASSOCIATED CONTENT

Comparison of the experimental spectra with theoretical calculations (Figure S1), CO oxidation rate in the temperature range of interest (Figure S2), Cu $L_{2,3}$-edges spectra of the high entropy oxide in the $CO+O_2$ mixture at temperatures below the starting of the CO oxidation reaction (Figure S3), Determination of the Cu(I) fraction (Figure S4 and Table S1), Discussion on the choice of soft-XAS as a mechanistic probe for the CO oxidation over the $Mg_{0.2}Co_{0.2}Ni_{0.2}Cu_{0.2}Zn_{0.2}O$ HEO, Details on the Powder X-ray Diffraction Analysis.

The following file is available free of charge: Supporting Info_rev.pdf.

AUTHOR INFORMATION

Notes

The authors declare no competing financial interests.

ACKNOWLEDGMENT

This work has been partially performed in the framework of the nanoscience foundry and fine analysis (NFFA-MIUR Italy Progetti Internazionali) project. The ELETTRA synchrotron radiation facility is thanked for provision of beamtime (exp. 20190091). The Italian ministry of University and Research is acknowledged for financial support through the PRIN 2107 program (project 2017KKP5ZR). Particular thanks are due to Dr. Primo Baldini (University of Pavia, Italy) for his help with the CO_2 sensor installation. V.C. thanks Prof. Angelo Sironi for fruitful discussions.

REFERENCES

1 Shelef, M.; McCabe, R. W. Twenty-five Years after Introduction of Automotive Catalysts: What Next? *Catal. Today* **2000**, *4*, 35–50.

2 Yoon, C.; Cocke, D. L. The Design and Preparation of Planar Models of Oxidation Catalysts: I. Hopcalite. *J. Catal.* **1988**, *113*, 2, 67–280.

3 Oh, S. H.; Hoflund, G. B. Low-Temperature Catalytic Carbon Monoxide Oxidation over Hydrous and Anhydrous Palladium Oxide Powders. *J. Catal*. **2007**, *245*, 35–44.

4 Date, M.; Okumura, M.; Tsubota, S.; Haruta, M. Vital Role of Moisture in the Catalytic Activity of Supported Gold Nanoparticles. *Angew. Chem. Int. Edn Engl.* **2004**, *43*, 2129–2132.

5 Yao, Y. Y. The Oxidation of Hydrocarbons and CO over Metal Oxides: III. Co_3O_4. *J. Catal*. **1974**, *33*, 108–122.

6 Grillo, F.; Natile, M. M.; Glisenti, A. Low-Temperature Oxidation of Carbon Monoxide: the Influence of Water and Oxygen on the Reactivity of a Co_3O_4 Powder Surface. *Appl. Catal.* B **2004**, *48*, 267–274.

7 Thormählen, P.; Skoglundh, M.; Fridell, E.; Andersson, B. Low-Temperature CO Oxidation over Platinum and Cobalt Oxide Catalysts. *J. Catal.* **1999**, *188*, 300–310.

8 Broqvist, P.; Panas, I.; Persson, H. A. DFT Study on CO Oxidation over Co_3O_4. *J. Catal.* **2002**, *210*, 198–206.

9 Jansson, J. Low-Temperature CO Oxidation over Co_3O_4/Al_2O_3. *J. Catal.* **2000**, *194*, 55–60.

10 Chen, H.; Fu, J.; Zhang, P.; Peng, H.; Abney, C. W.; Jie, K.; Liu, X.; Chi, M.; Dai, S. Entropy-stabilized Metal Oxide Solid Solutions as CO Oxidation Catalysts with High-Temperature Stability. *J. Mater. Chem. A* **2018**, *6*, 11129.

11 Rost, C. M.; Sachet, E.; Borman, T.; Moballegh, A.; Dickey, E. C.; Hou, D.; Jones, J. L.; Curtarolo, S.; Maria, J. P. Entropy-Stabilized Oxides. *Nat. Commun*. **2015**, *6*, 8485.

12 Sarkar, A.; Wang, Q.; Schiele, A.; Chellali, M. R.; Bhattacharya, S.S.; Wang, D.; Brezesinski, T.; Hahn, H.; Velasco, L.; Breitung, B. High-Entropy Oxides: Fundamental Aspects and Electrochemical Properties. *Adv. Mater.* **2019**, *31*, 1806236.

13 Frei, E.; Gaur, A.; Lichtenberg, H.; Heine, C.; Friedrich, M.; Greiner, M.; Lunkenbein, T.; Grunwaldt, J.-D.; Schlögl, R. Activating a Cu/ZnO:Al Catalyst – Much More than Reduction: Decomposition, Self-Doping and Polymorphism. *ChemCatChem* **2019**, *11*, 1587-1592.

14 Al Samarai, M.; Hahn, A. W.; Askari, A. B.; Cui, Y-T.; Yamazoe, K.; Miyawaki, J.; Harada, Y.; Rüdiger, O.; DeBeer, S. Elucidation of Structure-Activity Correlations in a Nickel Manganese Oxide Oxygen Evolution Reaction Catalyst by Operando Ni L-edge X-ray Absorption Spectroscopy and 2p3d Resonant Inelastic X-ray Scattering. *ACS Appl. Mater. Interfaces* **2019**, *11*, 38595-38605.

15 Wiese, K.; Abdel-Mageed, A. M.; Klyushin, A.; Behm, R. J. Dynamic Changes of Au/ZnO Catalysts during Methanol Synthesis: A Model Study by Temporal Analysis of Products (TAP) and Zn L_{III} near Edge X-ray Absorption Spectroscopy *Catal. Today* **2019**, *336*, 193-202.

16 Grioni, M.; Goedkoop J. B.; Schoorl, R.; de Groot, F. M. F.; Fuggle, J. C.; Schäfers, F.; Koch, E. E.; Rossi, G.; Esteva, J.-M.; Karnatak, R. C. Studies of Copper Valence States with Cu L_3 X-ray Absorption Spectroscopy. *Phys. Rev. B* **1989**, *39*, 1541-1544.

17 Wang, Y.; Lany, S.; Ghanbaja, J.; Fagot-Revurat, Y.; Chen, Y. P.; Soldera, F.; Horwat, D.; Mücklich, F.; Pierson, J. F. Electronic Structures of Cu_2O, Cu_4O_3, and CuO: A Joint Experimental and Theoretical Study. *Phys. Rev. B* **2016**, *94*, 245418.

18 Alders, D.; Tjeng, L. H.; Voogt, F. C.; Hibma, T.; Sawatzky, G. A.; Chen, C. T.; Vogel, J.; Sacchi, M.; Iacobucci, S. Temperature and Thickness Dependence of Magnetic Moments in NiO Epitaxial Films. *Phys. Rev. B* **1998**, *57*, 11623-11631.

19 Bora, D. K; Cheng, X.; Kapilashrami M.; Glans, P. A., Luo, Y.; Guo J.-H. Influence of Crystal Structure, Ligand Environment and Morphology on Co L-edge XAS Spectral Characteristics in Cobalt Compounds. *J. Synchrotron Radiat.* **2015**, *22*, 1450–1458.

20 Berardan, D.; Meena, A.K.; Franger, S.; Herrero, C.; Dragoe, N. Controlled Jahn-Teller distortion in (MgCoNiCuZn)O-based high entropy oxides *J. Alloys Compd.* **2017**, 704, 693-700

21 Rost, M. C.; Rak, Z.; Brenner, D. W.; Maria, J.-P. Local Structure of the $Mg_xNi_xCo_xCu_xZn_xO$ (x=0.2) Entropy-Stabilized Oxide: An EXAFS Study. *J. Am. Ceram. Soc.* **2017**, *100*, 2732-2738.

22 Shi, G.; Liu, J.; Chen, B.; Bao, Y.; Xu, J. Phase-Controlled Growth of Cubic Phase CuO Nanoparticles by Chemical Vapor Deposition. *Phys. Status Solidi A*. **2017**, *214*, 1700041.

23 Castán-Guerrero, C.; Krizmancic, D.; Bonanni, V.; Edla, R.; Deluisa, A.; Salvador, F.; Rossi, G.; Panaccione, G.; Torelli, P. A Reaction Cell for Ambient Pressure Soft X-ray Absorption Spectroscopy. *Rev. Sci. Instrum.* **2018**, *89*, 054101.

24 Abbate, M.; Goedkoop, J. B.; de Groot, F.M.F.; Grioni, M.; Fuggle, J.C.; Hofmann, S.; Petersen, H.; Sacchi, M. Probing Depth of Soft X-ray Absorption Spectroscopy Measured in Total-Electron-Yield Mode. *Surf. Interface Anal.* **1992**, *18*, 65–69.

25 Stavitski, E.; De Groot, F. M. F. The CTM4XAS Program for EELS and XAS Spectral Shape Analysis of Transition Metal L edges. *Micron* **2010**, *41*, 687-94.

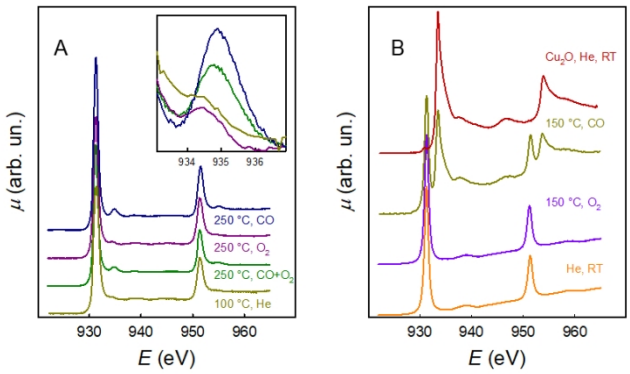

Figure 1 – A: Cu L2,3-edge XAS spectra of the Mg0.2Co0.2Ni0.2Cu0.2Zn0.2O HEO material in different conditions. The inset shows on an enlarged scale the Cu(I) peak at ca. 934.8 eV. B: Cu L2,3-edge XAS spectra of CuO in different conditions and of Cu2O at room temperature. In this panel, non-normalised spectra are shown

338x190mm (96 x 96 DPI)

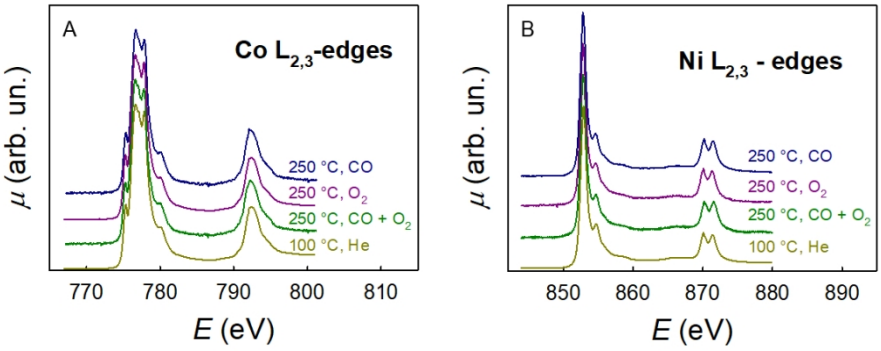

Figure 2 – A: Co L2,3-edge XAS spectra of the Mg0.2Co0.2Ni0.2Cu0.2Zn0.2O HEO material in different conditions. T. B: same as A but at the Ni L2,3-edge.

338x190mm (96 x 96 DPI)

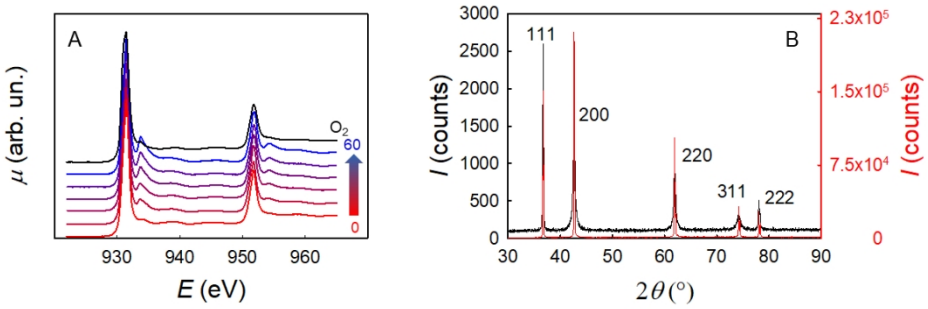

Figure 3 – A: Cu L2,3-edge XAS spectra of the Mg0.2Co0.2Ni0.2Cu0.2Zn0.2O HEO material for different time periods in CO at 235 °C (red to blue lines; numbers 0 □ 60 are the dwell times in these conditions expressed in minutes), and then in O2 at the same temperature (black line). B: comparison of the XRPD pattern of the raw HEO material (red line) and of the same material after all the thermal treatments described in this work (black line). The patterns are indexed according to the rock-salt structure.

338x190mm (96 x 96 DPI)